Theor Chem Acc (2000) 104:13–21
DOI 10.1007/s002149900100

Theoretical
Chemistry Accounts

Regular article

Does the topological approach characterize the hydrogen bond?

Franck Fuster, Bernard Silvi

Laboratoire de Chimie Théorique, Université Pierre and Marie Curie, 4 place Jussieu, F-75252 Paris Cedex 05, France

Received: 19 April 1999 / Accepted: 22 July 1999 / Published online: 17 January 2000

Abstract. The topological analysis of the electron localization function has been applied to complexes representative of the weak, medium and strong hydrogen bond. For both the weak and the medium hydrogen bonds, the number of basins in the complexes is the sum of those of the moieties. In this case, the formation of a weak or a medium hydrogen-bonded complex does not involve a chemical reaction. In the weak hydrogen bond case, the reduction of the localization domain yields two domains in the first step, which can be partitioned afterwards into valence and core domains. In contrast, for medium complexes the core–valence separation is the first event which occurs during the reduction process and therefore the complex should be considered as a single molecular species. Moreover, the analysis of the basin population variance indicates in this case a noticeable delocalization between the V(A, H) and V(B) basins. Finally, the symmetrical strong hydrogen bond has a protonated basin V(H) at the bond midpoint. Such a topology corresponds to an incomplete proton transfer and to a rather covalent bond.

Key words: Hydrogen bond – Electron localization function – Topological analysis – Population analysis – Delocalization

1 Introduction

The characterization of the hydrogen bond has given rise to a large number of experimental works as well as theoretical investigations in order to understand the energetics, the structures and the bonding properties of the complexes. According to energetic and spectroscopic criteria, the generally adopted classification of these complexes consists of three main classes, namely the weak, medium and strong hydrogen-bonded systems.

Correspondence to: B. Silvi
e-mail: silvi@lct.jussieu.fr

The hydrogen bond, symbolized by AH . . . B, results from the interaction between the proton donor AH and the proton acceptor B which can ultimately lead to the formation of the ionic pair $\{A^-, BH^+\}$. The weak hydrogen bond is characterized by an interaction energy of the order of 20 kJ mol^{-1} or less and by a frequency redshift of the ν_{AH} stretching mode of a few ten to a few hundred reciprocal centimetres. As typical examples of weakly hydrogen bonded systems we can mention the dimers and codimers of hydrogen halides, the water dimer and the complexes of hydrogen halides with water, carbon monoxide and rare gases. The FH. . .NH_3 complex is representative of the medium hydrogen bond: its complexation energy is -54.3 kJ mol^{-1} [1], whereas the ν_{FH} frequency shift is 746 cm^{-1}. Finally, the strong hydrogen bond, which is encountered in the solid state, generally involves dihalide anion HX_2^- units, such as in the crystalline phases of MHF_2, (M = Li, Na, K, Rb, Cs). In this case, the bond energy is over 100 kJ mol^{-1} [2, 3] and the frequency of the proton stretching mode lies in a region below 1600 cm^{-1} (i.e. the frequency shift rises 2000 cm^{-1}).

Though the energetic and spectroscopic criteria offer a clear demarcation between systems and suggest noticeable differences in their bonding properties, the different hydrogen-bonded systems have been treated on an equal footing in order establish correlations between their structures and their properties. The empirical laws derived in this spirit from the $\Delta\nu_{AH}/R_{A-B}$ [4] and the r_{AH}/R_{A-B} correlation curves [5, 6] testify this statement. These correlations are at the root of the "unified" phenomenological potentials (such as those of Lippincott and Schroeder [7], Lawrence and Robertson [8], Matsushita and Matsubara [9]) widely used to mimic the dynamics of the proton in numerical simulations. To establish such potentials, it is implicitly assumed that the different hydrogen bonds belong to the same kind of chemical bond; however, there is no experimental evidence and only quantum chemical calculations are able to provide qualitative and quantitative arguments to support (or not support) this interpretation.

The attention of quantum chemists has been mostly focused on two aspects of the calculation of hydrogen

bonds. On the one hand are technical problems dealing with the difficulty of obtaining reliable results. The interaction energy in the supermolecule approach is the difference of two huge quantities: the energy of the complex and the sum of the energies of the free species. Therefore, basis-set effects as well as the choice of the level of calculation are important. This point has been addressed in detail in the literature [10–18]. At the same time, numerical schemes allowing a significant improvement of the interaction energy have been proposed, such as the basis-set superposition error counterpoise correction [19–21]. On the other hand, a physical discussion of the contributions to the interaction energy can be made with the help of different partition schemes which basically rely on the antisymmetrized Rayleigh–Schrödinger perturbation ansatz [22–24]. Within these frameworks the interaction energy is written as the sum of electrostatic, induction, dispersion, exchange and penetration contributions.

To a lesser extent, the analysis of the wave function of the complexes has been studied in order to discuss the electrostatic or covalent character of the hydrogen bond. Such studies rely either on the valence bond approach [25] or on the projection of the charge density on atomic centres (population analysis) carried out with the Mulliken scheme [26–29] or with more elaborate techniques such as the Natural Bond Orbital (NBO) analysis [30, 31] in order to determine the magnitude of the electronic charge transfer between the proton donor and the proton acceptor units.

The electrostatic approach has been widely supported by the work of Buckingham and Fowler [32–34], who have shown that this contribution determines the geometry of the weakly bonded complexes. This interpretation, based on physical arguments, challenges another opinion commonly held by the chemistry community and originally formulated by Legon and Millen [35, 36] according to which the structure of hydrogen-bonded complexes is mostly driven by the location of the lone pair of the proton acceptor in the spirit of Gillespie's (VSEPR) model [37, 38]. The analysis of the electron charge density within the theory of "Atoms in molecules" (AIM) [39] provides a quantitative description of the electron redistribution as it enables the nucleophilic site of the base to be located [40, 41].

Neither the experimental nor the quantum chemical approach has been able to provide a clear answer to the question of the unicity of the hydrogen bond. This might be due to the lack of reliable tools to extract qualitative information from quantitative information. The advent of topological methods of analysis of local electronic functions [39, 42] offers the opportunity of reinvestigating the hydrogen bond. Here we present a series of analyses of the bonding carried out on complexes between FH and a series of proton acceptors, namely N_2, OCS, CO_2, CO, FH, HCN, SC, H_2, NH_3 and F^-, which covers a wide range of hydrogen-bond strengths. Moreover, symmetrical $H_5O_2^+$ and $N_2H_7^+$ species have been considered in order to verify the findings made on FHF^-. As will be shown, the topological analysis of the electron localization function provides unambiguous criteria to characterize each type of hydrogen bond.

2 Concepts and methodology

2.1 Résumé of the topological theory of the chemical bond

The partition of the molecular space into chemically significant regions still remains an open challenge and has been compared to the quest of the Holy Grail [43]. A natural way to achieve such a partition would be to express the Hamiltonian in terms of atomic and bonding contributions. This cannot be done directly because the potential-energy operator is not linear with respect to atomic centres. An alternative method projects this operator on the complete set of the atomic eigenfunctions [44], unfortunately yielding unphysical contributions to the energy.

The topological analysis of gradient dynamical systems was pioneered by Bader [39] in the case of the electron charge density gradient field (this constitutes the theory of AIM). Within this theory the molecular space is divided into adjacent nonoverlapping regions, the atomic basins, which have additive properties and which enable atomic charges to be rigorously defined. The discussion of the bonding made by Bader relies on the Laplacian of the charge density which provides electronic regions corresponding to those invoked by Gillespie in the VSPER model; however, the analysis of $\nabla^2\rho$ is not free of a drawbacks. For example, in the case of a few heavy atoms, it does not yield the expected number of shells; moreover, the physical reasons which justify the choice of the charge density Laplacian are not fully convincing. In 1990, Becke and Edgecombe [45] proposed a local scalar function, the electron localization function (ELF) denoted by $\eta(r)$, which is related to the Fermi hole curvature. As shown by Savin et al. [46] the ELF measures the excess kinetic energy density due to the Pauli repulsion. In the region of space where the Pauli repulsion is weak (single electron or opposite spin-pair behaviour) the ELF is close to unity, whereas where the probability to find the same-spin electrons close together is high the ELF tends to zero.

As the ELF is a scalar function, the analysis of its gradient field can be carried out in order to locate its attractors (the local maxima) and the corresponding basins. The picture of the molecule provided by the ELF analysis [42] is consistent with the Lewis valence theory [47] and therefore it is possible to assign a chemical meaning to the attractors and to their basins. There are basically two chemical types of basins: the core basins labelled by C(atom symbol), which encompass nuclei with $Z > 2$, and the valence basins, V(list of atoms). These latter are characterized by their synaptic order, which is the number of core basins with which they share a common boundary. A proton located in a valence basin is counted as a formal core and thus increases the synaptic order by 1. Accordingly, a basin may be mono-, di or polysynaptic corresponding to lone-pair, bicentric and polycentric bonding regions, respectively [48]. For example, ammonia has one core basin, C(N), one monosynaptic basin, V(N), and three protonated disynaptic basins, V(N, H_i).

Graphical representations of the bonding are obtained by plotting isosurfaces of the localization function which delimit volumes within which the Pauli repulsion is rather weak. The localization domains are called irreducible when they contain only one attractor and are called reducible otherwise. The reduction of reducible domains is another criterion of discrimination between basins. The reduction of a reducible localization domain occurs at a critical value of the bounding isosurface, over which the domain is split into domains containing fewer attractors. The localization domains are then ordered with respect to the ELF critical values, yielding bifurcations. Starting at a very low ELF value, we find only one localization domain [the whole space for $\eta(\mathbf{r}) = 0$]. Upon increasing the isosurface-defining value, we meet a first separation between valence and core domains. At higher ELF values the valence reducible domain is split in turn. The hierarchy of the bifurcation can be visualized by a tree diagram.

Beyond these qualitative aspects, the partition of the molecular space enables basin-related properties to be calculated by integrating a given density of the property over the volume of the basins. Of particular interest are the basin population

$$\bar{N}(\Omega_i) = \int_{\Omega_i} \rho(\mathbf{r}) d\mathbf{r} \tag{1}$$

and its variance

$$\sigma^2(\bar{N};\Omega_i) = \int_{\Omega_i} \pi(\mathbf{r}_1,\mathbf{r}_2) d\mathbf{r}_1 d\mathbf{r}_2 - \bar{N}(\Omega_i)[\bar{N}(\Omega_i) - 1] \ , \tag{2}$$

in which $\pi(\mathbf{r}_1,\mathbf{r}_2)$ is the two-electron density. Both the basin population and the variance are observables in the sense of quantum mechanics as they can be expressed as expectation values of operators. In contrast, the variance square root, classically the standard deviation, has no physical meaning. The variance can be expressed as the sum of contributions arising from the other basins [49]:

$$\sigma^2(\bar{N};\Omega_i) = \sum_{j\neq 1} \bar{N}(\Omega_i)\bar{N}(\Omega_j) - \int_{\Omega_i}\int_{\Omega_j} \pi(\mathbf{r}_1,\mathbf{r}_2) d\mathbf{r}_1 d\mathbf{r}_2 \times \sum_{j\neq 1} C(\Omega_i,\Omega_j) \ . \tag{3}$$

The variance is a measure of the quantum mechanical uncertainty of the basin population, which can be interpreted as a consequence of the electron delocalization, whereas the pair covariance indicates how much the population fluctuations of two given basins are correlated.

The topological analysis of the ELF gradient field also provides a tool for the study of the evolution of the bonding along a reaction pathway [50]. In the topological context, the transformation of the bonding is expressed by the appearance and disappearance of local maxima, which can be studied with the help of Thom's catastrophe theory [51].

2.2 What can be learnt from the topological approach?

Considering the hydrogen-bond formation from the AH and B fragments we predict that only four different topological patterns may exist for the complex:

1. The topology of AH...B is just the addition of those of the moieties. There is neither a change in the number of basins nor in their synaptic order. In the reduction of the localization process the first bifurcation creates two molecular reducible domains, one for AH the other for B, for a value defining the bounding isosurface lower than that of the core–valence separation.
2. The same as in case 1, except that the core–valence separation is the first bifurcation occurring in the reduction of the localization. In this case the complex can be viewed as a single molecule.
3. The V(A, H) disynaptic basin has been split into two monosynaptic ones, V(A) and V(H) as has been evidenced in proton-transfer reactions [52, 53].
4. The proton transfer is completed; the basins are now V(A) and V(B, H).

Physically case 1 corresponds to the electrostatic interaction of the partners, whereas case 2 implies an additional interaction which can be due to the electronic delocalization between the V(A, H) and V(B) basins. These two patterns are therefore expected to be the topological signatures of the weak and medium hydrogen-bond classes, respectively. Symmetric strong hydrogen bonds are consistent with the topology of case 3 and finally case 4 must be considered as an ionic pair rather than as a hydrogen-bonded complex.

In order to build up a scale for the weak and medium hydrogen bonds based on topological criteria we define the core–valence bifurcation (CVB) indices as the difference of $\eta(\mathbf{r}_{cv})$, the lowest value of the ELF for which all the core basins of the complex are separated from the valence, and $\eta(\mathbf{r}_{AHB})$, the value at the saddle connection of the V(A, H) and V(B) basins. The CVB indices denoted hereafter by ϑ(AHB) are expressed as

$$\vartheta(\mathrm{AHB}) = \eta(\mathbf{r}_{cv}) - \eta(\mathbf{r}_{\mathrm{AHB}}) \ . \tag{4}$$

The CVB index is positive for the weak interaction of case 1 and negative for the medium hydrogen bond in which the complex is a single molecular species. It should be emphasized that the $(3,-1)$ critical point of the ELF gradient field used to define ϑ(AHB) coincides with the hydrogen bond critical point which plays a central role in the criteria for hydrogen bonding proposed by Koch and Popelier [54].

According to Eq. (3), the pair covariance of the V(A, H) and V(B),

$$C(\mathrm{AH,B}) = \bar{N}[\mathrm{V(A,H)}]\bar{N}[\mathrm{V(B)}] - \int_{\mathrm{V(A,H)}}\int_{\mathrm{V(B)}} \pi(\mathbf{r}_1,\mathbf{r}_2) d\mathbf{r}_1 d\mathbf{r}_2 \ , \tag{5}$$

is a measure of the delocalization between the proton donor and the proton acceptor. This quantity, which is related to the delocalization contribution introduced by Coulson [55] in the partition of the interaction energy, is expected to increase as the CVB index decreases.

Quantitatively, the formation of the hydrogen bond would induce intramolecular and intermolecular charge transfers due to electrostatic polarization effects and to electron delocalization between the V(A, H) and V(B) basins, respectively. In all cases, the V(B) basin population is expected to decrease for the benefit of the other valence basins of B and more precisely for those sharing a boundary with V(B). In the case of a noticeable intermolecular charge transfer, the valence basins of B would also gain electron density at the expense of V(B). The localization in the protonated basin, V(A, H), is higher than in the monosynaptic one, V(B), as a local maximum of the electron density is located on the proton due to its Coulomb attractive potential. The V(A, H) basin exerts a "pressure" over V(B) which tends to lower the localization within it and therefore the value of the ELF at its attractor. The same trend, but with a smaller amplitude, would also occur for V(A, H).

3 Results and discussion

3.1 Method of calculation

The calculations were performed in order to confirm (or invalidate) the hypothesis made in the previous section on the basis of the general properties of the localization basins. A faithful representation of the complexes with respect to experiment is not a critical requirement for this purpose. Indeed what is needed is a self-consistent set of results obtained with the same level of calculation and with basis functions of homogeneous quality. Moreover, at the present state of the art the calculation of the variance of the basin population which is necessary to carry out the analysis of the delocalization dictates that the wave function is expressed in terms of a single determinant built on Hartree–Fock or Kohn–Sham spin orbitals. The hybrid Hartree–Fock/density functional method Becke3LYP [56–59] appears to be a reasonable compromise, though not fully satisfactory. On the one hand, it takes care of the Coulomb hole–electron correlation and, on the other hand, it provides a better description of the exchange in the intermolecular region than the pure density functional theory approaches based on the local density approximation or the generalized gradient approximation. The Becke3-LYP scheme used in conjunction with the 6-31G(d,p) basis set [60–62] provides reasonable geometries for complexes in which HF is the proton donor as well as realistic dissociation energies and harmonic frequency

shifts of the FH stretching mode. The ab initio calculations were performed with the Gaussian94 software [63]. For the weak and medium hydrogen-bonded complexes the structures were fully optimized and the vibrational frequencies were calculated at the harmonic level. The counterpoise correction [19] was applied to evaluate the dissociation energies. The geometry optimizations of FHF^-, $H_5O_2^+$ and $N_2H_7^+$ were carried out with $D_{\infty h}, C_{2h}$ and D_{3h} symmetry constraints, respectively.

3.2. Topological analysis of the monomeric species

The localization domains of the monomeric species involved in the hydrogen-bonded complexes are displayed in Fig. 1. For a given value of the bounding isosurface their shapes provide a qualitative picture of the VSEPR electron-pair domains. Typically, in agreement with the VSEPR assumptions, the lone pairs (here the monosynaptic domains in orange) occupy more space than bonds (disynaptic domains in green) except for those with hydrogen (protonated disynaptic in blue) which have a size comparable to that of lone pairs. The relative sizes of the localization domains are not proportional to the corresponding basin populations, for example, in the carbon monoxide molecule the V(C) domain is larger than the V(O) one though the population of the latter is roughly twice that of the former basin. As a general rule, the largest monosynaptic domains belong to the most electropositive centre. The partition of the hydrogen fluoride molecular space gives rise to three basins as illustrated in Fig. 1: the fluorine atom core, C(F), the lone pairs gathered in a single basin, V(F), by the cylindrical symmetry and the V(F, H) disynaptic basin. The populations of these basins are 2.14*e*, 6.55*e* and 1.30*e*, respectively. The structure of FH is essentially covalent though a noticeable electron transfer of about 0.5*e* from V(F, H) towards V(F) indicates a strong polarization of the FH bond. Moreover, the pair covariance, C[V(F), V(F, H)], is rather large (0.72), which is an indication of a noticeable electron delocalization within the valence shell. It is worth noting that the formation of an ionic pair involving a bare proton is not physically possible because the proton essentially behaves as a strong attractive Coulombic potential on the electron density without the Pauli repulsive counterpart arising from core shells. The localization domain reduction tree diagram is presented in Fig. 2.

The electrophilic valence basin populations of the proton acceptor molecules ordered according to the calculated hydrogen-bond strength in their complexes with HF are summarized in Table 1. Let us first consider N_2 and NH_3 (Fig. 1), which are the acceptors in the weakest ($FH\ldots N_2$) and the strongest ($FH\ldots NH_3$) complexes investigated in the present study. The topological representation of N_2 shows two core basins, $C(N_1)$ and $C(N_2)$, two monosynaptic basins, $V(N_1)$ and $V(N_2)$, and the disynaptic basin $V(N_1, N_2)$ between the two cores. The population in this last basin is only 3.34*e*, about half of what is expected from the standard Lewis

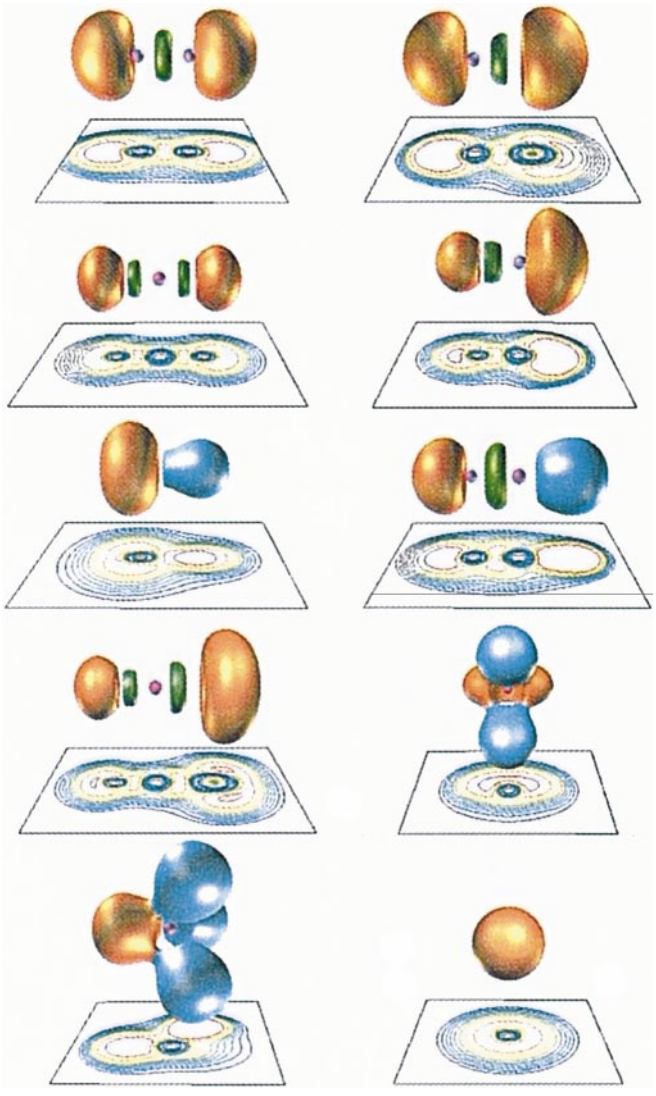

Fig. 1. Localization domains and contour maps of $\eta(r)$ for the monomers. From *left* to *right* and from *top* to *bottom*: N_2, SC, CO_2, CO, FH, HCN, SCO, H_2O, NH_3 and F^-. The colour code used for the localization domain is core: *magenta*, valence monosynaptic: *orange*, valence protonated: *blue*, valence disynaptic: *green*. The spacing of the isovalues is 0.1; the external contour corresponds to $\eta(r) = 0.1$ steps of 0.1

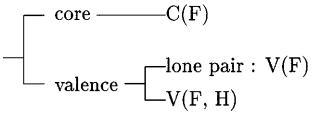

Fig. 2. Localization domain reduction tree diagram of FH

representation |N≡N|. As a consequence of the weakness of the N—N bond the nitrogen lone pairs $V(N_1)$ and $V(N_2)$ have rather large populations (i.e. 3.22*e*, instead of about 2*e*). Moreover, there is a significant delocalization between the $V(N_i)$ and the $V(N_1, N_2)$ basin, which is reflected by a pair covariance of 0.60. In NH_3, the population of the C(N) core basin of 2.12*e* is identical to that calculated for N_2. The three $V(N, H_i)$ disynaptic basins also have populations close to the

Table 1. Electrophilic basin population and total valence-shell population of the proton donor/acceptor molecules

Molecule	V(B)		
	Centre	$\bar{N}$[V(B)]	Total valence
N_2	N	3.22	9.78
CO_2	O	4.90	15.62
SCO	O	4.70	15.70
CO	C	2.58	9.77
HF	F	6.55	7.85
HCN	N	3.04	9.81
SC	C	2.57	9.87
H_2O	O	2.22	7.84
NH_3	N	2.15	7.88

Lewis expectation (i.e. 1.91*e*), whereas the electron transfer towards V(N) should be weak since the V(N) population is 2.15*e*, close to the value of a conventional lone pair. In this molecule, the V(N) monosynaptic basin is less involved in the delocalization within the valence shell than in N_2. The localization domain reduction tree diagrams of N_2 and NH_3 are given in Figs. 3 and 4, respectively.

It should be noted that for a given atom B, the populations of the V(B) electrophilic basins follow an order opposite to that of the hydrogen-bond strength in the complexes. This is true for the N_2, HCN, NH_3 triad, for CO and SC and for CO_2, SCO and H_2O.

3.3 The weak and medium hydrogen-bonded complexes

Figure 5 displays the ELF plot of the FH...N_2, FH...OCS, FH...CO_2, FH...CO, FH...FH, FH...NCH, FH...CS and FH...NH_3 complexes, whereas the most significant quantitative information, namely the CVB indices, the V(B) population variation, the basin pair covariance C[V(B), V(F, H)], the net population transfer, the counterpoise-corrected complexation energies and the ν_{FH} harmonic frequency shifts, is reported in Table 2. The hydrogen-bond formation noticeably reduces the volumes of the V(A, H) and V(B) localization domains with respect to the uncomplexed species. Their mutual Pauli repulsion in

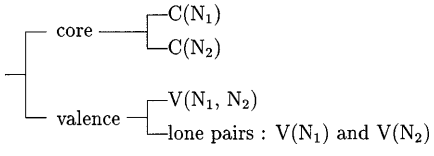

Fig. 3. Localization domain reduction tree diagram of N_2

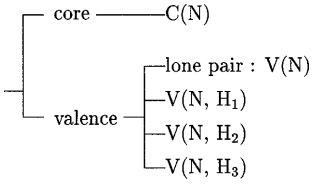

Fig. 4. Localization domain reduction tree diagram of NH_3

the complex flattens their opposite bounding isosurfaces. This effect can be viewed as the consequence of the fourth and eighth rules of Koch and Popelier [54] on the ELF gradient field, i.e. the mutual penetration of the hydrogen and acceptor atom and the decrease in the hydrogen atom volume. The patterns displayed by the contour maps clearly show the competition between the valence domain and the core–valence separations.

As expected there are two qualitative behaviours which are exemplified by the FH...N_2 and FH...NH_3 complexes. The localization domain reduction diagram of the FH...N_2 complex, which corresponds to the weakest interaction as indicated by the values of the complexation energy, the frequency shift and the CVB index is shown in Fig. 6. As ϑ(FHB) is negative the first bifurcation splits the parent irreducible domain into two molecular domains corresponding to the FH and N_2 moieties. The core–valence separation occurs at a higher value of the ELF as shown in Fig. 7: the lowest value of $\eta(\mathbf{r})$ is located at the saddle point of index 1 on the separatrix of the V(F, H) and V(N) basins. Clearly the formation of a weak hydrogen-bonded complex changes neither the number of basins nor the type of the basins. It simply adds the critical points of each partner and provides the saddle points necessary to fulfil the Poincaré–Hopf relationship. Moreover, each moiety keeps its individual valence shell. The qualitative changes are therefore subtle. On the one hand, the $\eta(\mathbf{r})$ values at the V(F, H) and V(N) attractors are lowered by a very small amount (0.001 and 0.003, respectively), which can be simply explained by the fact that in a closed-shell system any approach to a localization domain by another localization domain increases the same spin-pair probability, at least in-between the attractors and, therefore, yields a narrowing of the Fermi hole at the attractor. With respect to the isolated monomeric species, the FH valence basin populations do not vary, whereas as on the nitrogen side the V(N_1, N_2) basin population is increased by 0.002*e* transferred from the V(N) basin in front of V(F, H). This charge transfer is due to the polarization of the N_2 subunit by the electric field of the proton donor. These results are consistent with the AIM analysis of Carroll et al. [40], who found a very small charge transfer (0.0046*e*) for this complex. The pair covariance, C[V(N), V(F, H)], is small.

In the case of the FH...NH_3 complex, the localization domain reduction first separates the core domains from the valence ones as shown in Fig. 8. The profile of $\eta(\mathbf{r})$ along the F-N direction displayed in Fig. 9 clearly shows that the value of the localization function on the core–valence separatrices of both the FH and NH_3 moieties is lower than that of the critical point of the V(N)-V(F, H) boundary by about 0.1. The most important change in the basin population occurs for V(N), the population of which is decreased by 0.1*e* with respect to free ammonia. This loss is distributed half to the V(F) basin and half to the V(N, H) basins. The net charge transfer is 0.04*e* towards the proton donor, in agreement with the findings of Ref. [40]. With respect to the FH...N_2 complex, as there is a single valence shell, the delocalization between the V(N) and V(F, H) basins is more than twice as large.

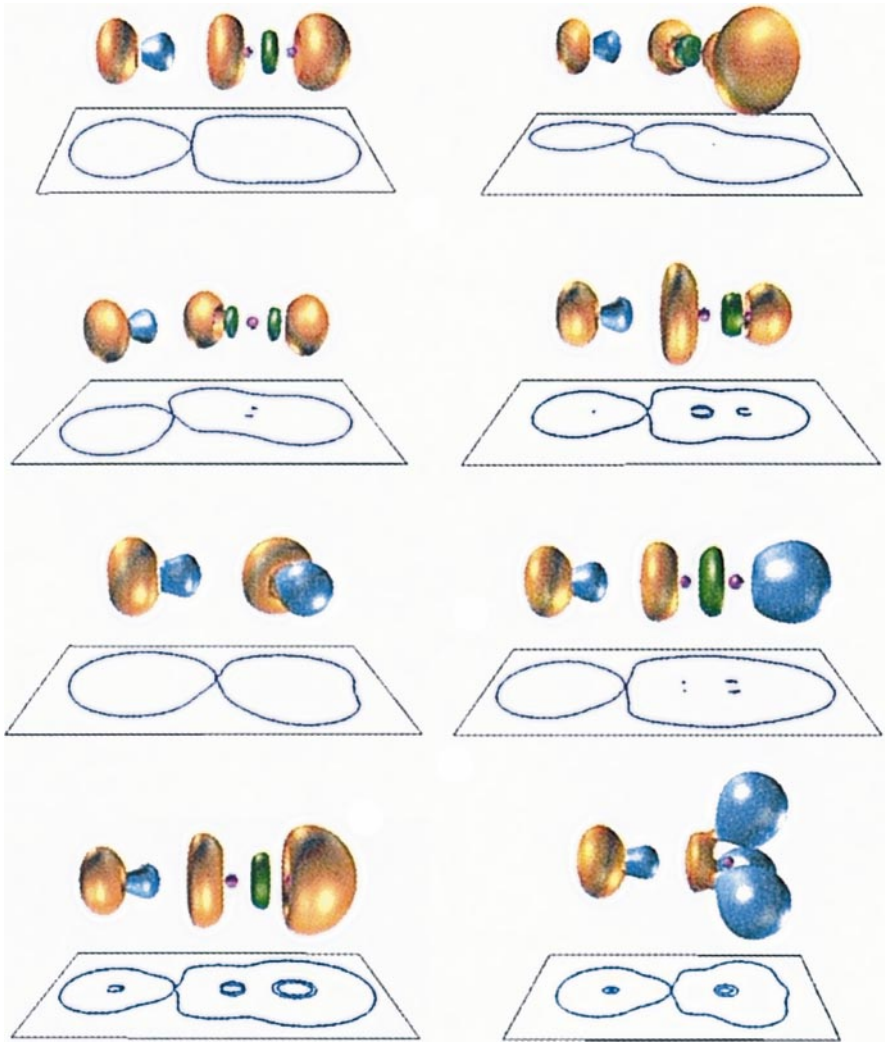

Fig. 5. Localization domains and contour maps of $\eta(r)$ for the weak and medium hydrogen-bonded complexes. From *left* to *right* and from *top* to *bottom*: FH...N_2, FH...OCS, FH...CO_2, FH...CO, FH...FH, FH...NCH, FH...CS and FH...NH_3. The colour code used for the localization domain is core: *magenta*, valence monosynaptic: *orange*, valence protonated: *blue*, valence disynaptic: *green*. The isocontour value is that of the saddle connection between the V(A, H) and V(B) basins, $\eta(r_{AHB})$. The core–valence separation is only achieved for FH...CS and FH...NH_3

Table 2. Core–valence bifurcation index, ϑ(FHB), ΔV(B) population variation (e), C[V(B), V(F, H)], net population transfer, ΔN(a.u.), complexation energies, D_e (kJ mol^{-1}), and FH stretching frequency shift, $\Delta\omega$, of the weak and medium hydrogen-bonded complexes

Acceptor	ϑ(FHB)	ΔV(B)	C[V(B), V(F, H)]	ΔN	D_e	$\Delta\omega$
N_2	−0.063	−0.02	0.028	0.0	7.6	−33
CO_2	−0.056	0.04	0.028	0.0	9.6	−27
SCO	−0.049	0.10	0.026	0.0	10.1	−29
CO	−0.025	−0.02	0.046	−0.02	13.7	−131
HF	−0.006	−0.01	0.038	−0.01	21.1	−143
HCN	0.001	−0.02	0.029	−0.01	26.4	−185
SC	0.002	−0.02	0.056	−0.03	27.5	−284
H_2O	0.018	−0.05	0.030	−0.01	36.6	−362
NH_3	0.083	−0.10	0.063	−0.04	54.6	−617

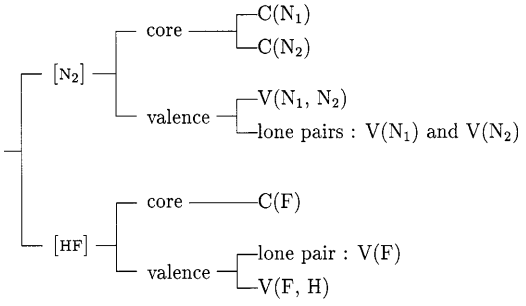

Fig. 6. Localization domain reduction tree diagram of FH...N_2

Among the complexes presented in Table 2, those with a negative CVB index behave as FH... N_2, whereas the remaining complexes behave as FH...NH_3. In all cases the V(F, H) basin population is identical in the complex and in the free monomer. A net electron transfer from the proton acceptor towards the proton donor occurs in the complexes between HF and CO, HF, HCN, SC, H_2O and NH_3. The magnitude of this transfer is very weak (0.01–0.04e and the values provided by the ELF analysis are in good agreement with those of the AIM analysis [40]. The net effect of the intermolecular charge transfer is to increase the V(F) population. The intermolecular transfer is due to an electron loss in the V(B) basin, which also participates in the polarization of the proton acceptor molecule as already mentioned in the FH... NH_3 case. The complexes

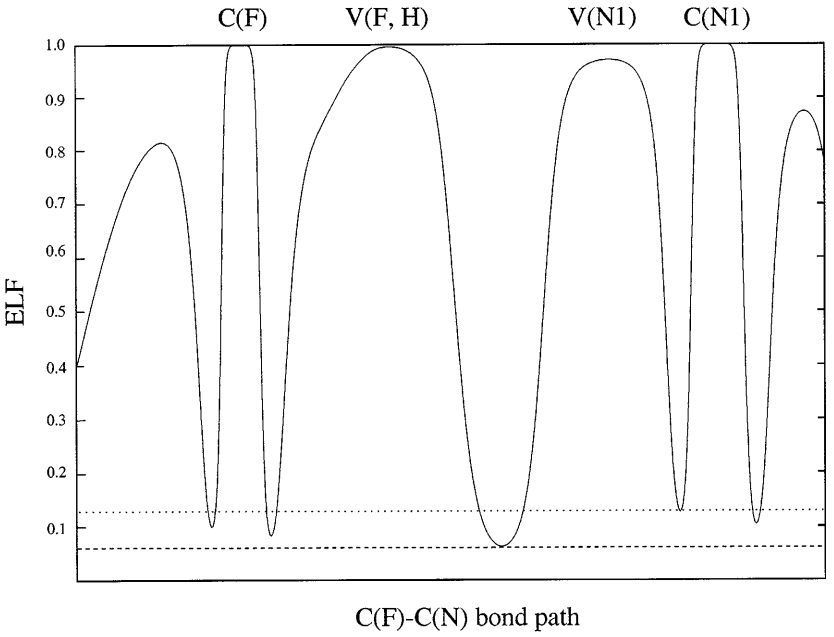

Fig. 7. $\eta(r)$ value along the bond path of the FH...N_2 molecule

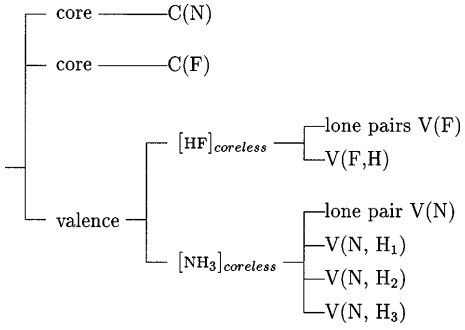

Fig. 8. Localization domain reduction tree diagram of $FH...NH_3$

involving the triatomic molecules CO_2 and SCO are the only ones in which the V(B) population is increased upon complexation. The electron transfer towards V(B) is made at the expense of the adjacent V(C, O) disynaptic basin, inducing as a consequence lengthening of the CO bond.

The calculated complexation energies and the frequency shifts are displayed in Figs. 10 and 11 as functions of the CVB indices. In both cases there is a good correlation, which justifies the use of the CVB index as a quantitative topological criterion. Hence, the topological and the experimentalist's criteria form consistent and complementary tools for the characterization of the hydrogen-bond strength.

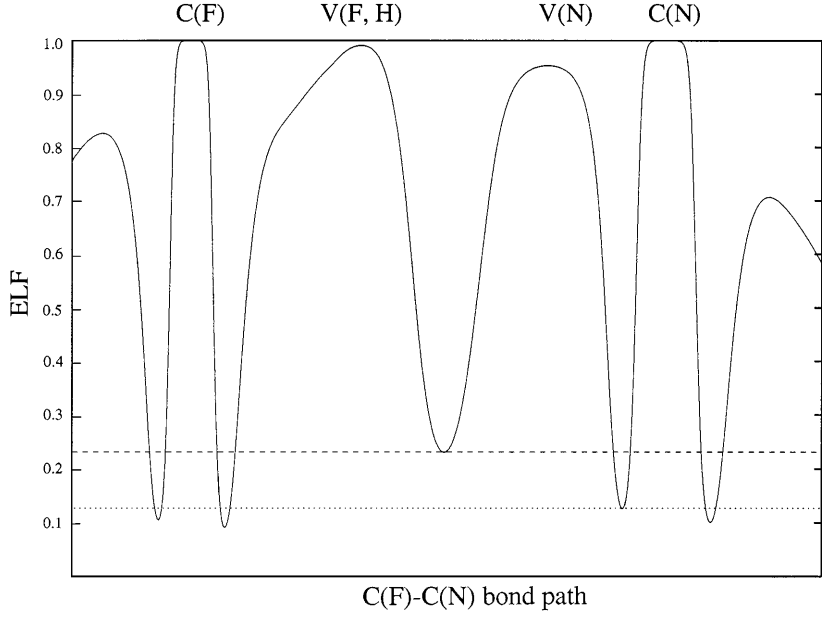

Fig. 9. $\eta(r)$ value along the bond path of the $FH...NH_3$ molecule

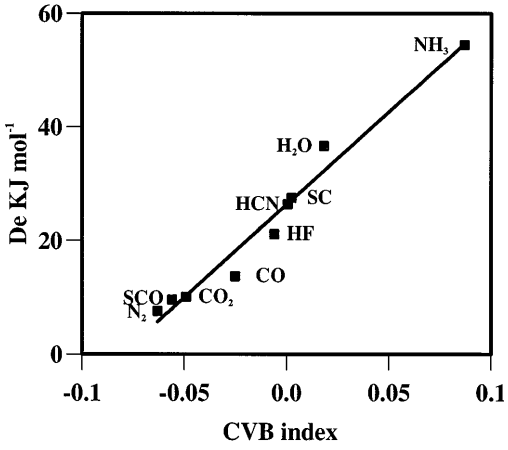

Fig. 10. Complexation energy versus core–valence bifurcation (*CVB*) indices

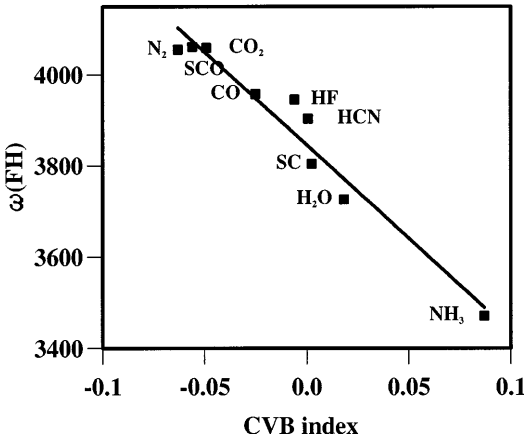

Fig. 11. FH stretching harmonic frequency shift (cm^{-1}) versus CVB indices

3.4 Strong hydrogen bond

The ELF gradient dynamical system of FHF^- (Fig. 12) contains five valence basins: two large monosynaptic basins, $V_1(F_1)$ and $V_1(F_2)$, whose attractors are degenerate on a circle due to the $D_{\infty h}$ symmetry of the anion, a protonated monosynaptic basin, V(H), centred at the F-F midpoint and two small monosynaptic basins, $V_2(F_1)$ and $V_2(F_2)$, between the fluorine core basins and V(H). The ELF value at the attractor of V(H) is lower than that of the V(F, H) attractor, 0.954 instead of 0.997. Moreover, the V(H) population is very small, 0.3*e*. The pair covariance, $C[V(H), V_2(F_1)]$, of 0.10 indicates a noticeable delocalization between V(H) and $V_2(F_i)$. This picture of the bonding has been previously encountered in the study of the proton-transfer reaction [52, 53], and it corresponds to the "topological transition state" in which the proton is detached from the reactant side and is not already attached on the product side. This topology is characteristic of the symmetrical strong hydrogen bond and can also be found in Fig. 12 in the $H_5O_2^+$ and $N_2H_7^+$ cases. Within the ELF topological framework the symmetrical strong hydrogen bond appears to be a true chemical bond since the topology of the complex is not the sum of the topologies of the proton donor and of the proton acceptor, as testified by the advent of the V(H) monosynaptic basin.

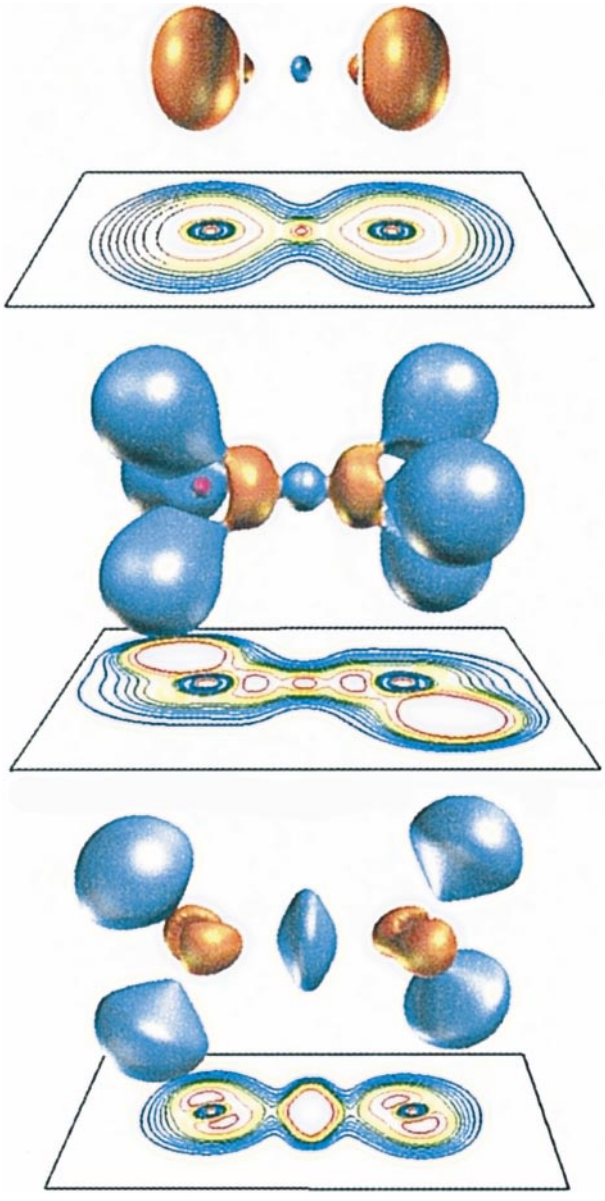

Fig. 12. Localization domains and contour maps of $\eta(r)$ for the strong hydrogen bond. From *top* to *bottom* FHF^-, $N_2H_7^+$ and $H_5O_2^+$. The colour code used for the localization domain is core: *magenta*, valence monosynaptic: *orange*, valence protonated: *blue*, valence disynaptic: *green*. The spacing of the isovalues is 0.1; the external contour corresponds to $\eta(r) = 0.1$ steps of 0.1

4 Conclusion

The topological analysis of the gradient dynamical system of the ELF function provides unambiguous criteria to distinguish weak, medium and strong interactions, at least on model hydrogen-bonded complexes. The weak interaction is not a chemical interaction since

the proton donor and proton acceptor molecules keep their individuality. The topology of the interaction can be sketched by the following model:

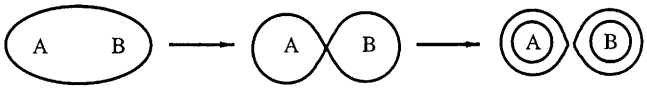

The topology of the medium-strength complex is rather similar to the weak case: the pattern results from the addition of the monomer plus the necessary saddle point of index 1, which ensures the preservation of the Poincaré–Hopf law; however, the proton donor and proton acceptor parts now belong to the same molecule since there is only one valence shell. The complexation process, though it is not a chemical reaction characterized either by a change in the number of basins or/and of the synaptic orders yields nevertheless a species which can be considered as a molecule on the basis of the topological criteria. Such a process is schematized by

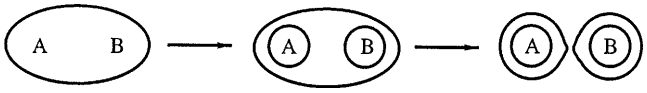

Finally, the strong symmetrical hydrogen bond can be represented by

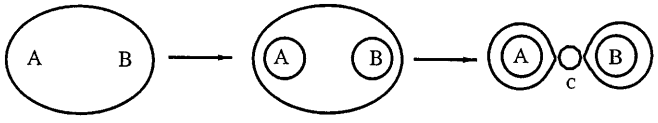

which corresponds to the formation of a new molecule by a chemical reaction. This reaction is the incomplete proton transfer which consists of the breaking of the covalent AH bond without the formation of the HB bond.

References

1. Szczęśniak MM (1984) J Phys Chem 88: 5923
2. Tuck DG (1968) Prog Inorg Chem 9: 161
3. Emsley J (1980) Chem Soc Rev 9: 91
4. Pimentel GC, MacClellan AL (1960) The hydrogen bond. Reinhold, San Francisco
5. Olovsson I, Jönson PG (1976) In: Schuster P, Zundel E, Sandorfy C (eds) The hydrogen bond. Recent developments in theory and experiments, vol II. North-Holland, Amsterdam, p 1426
6. Ichikawa M (1978) Acta Crystallogr Sect B 34: 2074
7. Lippincott ER, Schroeder R (1955) J Chem Phys 23: 1099
8. Lawrence MC, Robertson GN (1987) J Chem Phys 87: 3375
9. Matsushita E, Matsubara T (1982) Prog Theor Phys 67: 1
10. Scheiner S (1991) In: Lipkowwitz KB, Boyd DB (eds) Computational chemistry. VCH, New York, pp 165–218
11. Latajka Z, Scheiner S (1984) J Chem Phys 81: 407
12. Latajka Z, Scheiner S (1987) Chem Phys Lett 140: 339
13. Latajka Z, Scheiner S (1987) J Chem Phys 87: 1194
14. Latajka Z, Scheiner S (1987) J Comput Chem 8: 663
15. Latajka Z, Scheiner S (1988) Chem Phys 122: 413
16. Latajka Z, Ratajczak H, Person WB (1989) J Mol Struct 194: 89
17. Latajka Z, Scheiner S, Chatasinski G (1992) Chem Phys Lett 196: 384
18. Latajka Z, Bouteiller Y, Scheiner S (1995) Chem Phys Lett 234: 159
19. Boys SF, Bernerdi F (1970) Mol Phys 19: 553
20. van Duijneveldt-van de Rijdt JGCM, van Duijneveldt FB (1997) In: Hadži D (ed) Theoretical treatments of hydrogen bonding. Wiley, Chichester, chapter 2, pp 13–47
21. Kolos W (1979) Theor Chim Acta 551: 219
22. Kitaura K, Morokuma K (1976) Int J Quantum Chem 10: 325
23. Claverie P (1978) In: Pullman B (ed) Intermolecular interactions: from diatomics to biopolymers. Wiley, New York, pp 69–286
24. Salewicz K, Jeziorski B (1979) Mol Phys 38: 191
25. Coulson CA (1952) Valence. Clarendon, Oxford
26. Mulliken RS (1955) J Chem Phys 23: 1833
27. Mulliken RS (1955) J Chem Phys 23: 1841
28. Mulliken RS (1955) J Chem Phys 23: 2338
29. Mulliken RS (1955) J Chem Phys 23: 2343
30. Reed AE, Weinstock RB, Weinhold F (1985) J Chem Phys 83: 735
31. Reed AE, Curtiss LA, Weinhold F (1988) Chem Rev 88: 899
32. Buckingham AD, Fowler PW (1983) J Chem Phys 79: 6425
33. Buckingham AD, Fowler PW, Stone AJ (1986) Int Rev Phys Chem 5: 107
34. Buckingham AD (1997) In: Hadži D (ed) Theoretical treatments of hydrogen bonding. Wiley, Chichester, chapter 2, pp 1–12
35. Legon AC, Millen DJ (1986) Chem Rev 86: 635
36. Legon AC, Millen DJ (1982) Discuss Faraday Soc 73: 61
37. Gillespie RJ, Robinson EA (1996) Angew Chem Int Ed Engl 35: 495
38. Bader RFW, Gillespie RJ, MacDougall PJ (1988) J Am Chem Soc 110: 7329
39. Bader RFW (1990) Atoms in molecules: a quantum theory. Oxford University Press, Oxford
40. Carroll MT, Chang C, Bader RFW (1988) Mol Phys 63: 387
41. Carroll MT, Bader RFW (1988) Mol Phys 65: 695
42. Silvi B, Savin A (1994) Nature 371: 683
43. Bachrach SM (1994) In: Lipkowwitz KB, Boyd DB (eds) Reviews in computational chemistry. VCH, New York, pp 171–227
44. Mayer I (1983) Int J Quantum Chem 23: 341
45. Becke AD, Edgecombe KE (1990) J Chem Phys 92: 5397
46. Savin A, Becke AD, Flad J, Nesper R, Preuss H, von Schnering HG (1991) Angew Chem Int Ed Engl 30: 409
47. Lewis GN (1966) Valence and the structure of atoms and molecules. Dover, New York
48. Savin A, Silvi B, Colonna F (1996) Can J Chem 74: 1088
49. Noury S, Colonna F, Savin A, Silvi B (1998) J Mol Struct 450: 59
50. Krokidis X, Noury S, Silvi B (1997) J Phys Chem A 101: 7277
51. Thom R (1972) Stabilité structurelle et morphogénèse. Intereditions, Paris
52. Krokidis X, Goncalves V, Savin A, Silvi B (1998) J Phys Chem A 102: 5065
53. Krokidis X, Vuilleumier R, Borgis D, Silvi B (1999) Mol Phys 96: 265
54. Koch U, Popelier PLA (1995) J Phys Chem 99: 9747
55. Coulson CA (1957) Research 10: 149
56. Becke AD (1993) J Chem Phys 98: 5648
57. Becke AD (1988) Phys Rev A 38: 3098
58. Lee C, Yang Y, Parr RG (1988) Phys Rev B 37: 785
59. Miechlich B, Savin A, Stoll H, Preuss H (1989) Chem Phys Lett 157: 200
60. Hehre WJ, Ditchfield R, Pople JA (1972) J Chem Phys 56: 2257
61. Clark T, Chandrasekhar J, Spitznagel GW, Schleyer PVR (1983) J Comput Chem 4: 294
62. Frisch MJ, Pople JA, Binkley JS (1984) J Chem Phys 80: 325
63. Frisch MJ, Trucks GW, Schlegel HB, Gill PMW, Johnson BG, Robb MA, Cheeseman JR, Keith T, Petersson GA, Montgomery JA, Raghavachari K, Al-Laham MA, Zakrzewski VG, Ortiz JV, Foresman JB, Cioslowski J, Stefanov BB, Nanayakkara A, Challacombe M, Peng CY, Ayala PY, Chen W, Wong MW, Andres JL, Replogle ES, Gomperts R, Martin RL, Fox DJ, Binkley JS, Defrees DJ, Baker J, Stewart JP, Head-Gordon M, Gonzalez C, Pople JA (1995). Gaussian 94, Revision D.4. Gaussian, Pittsburgh, Pa